

Analytical Characterization of Common-mode Voltage in A Three-level ANPC Inverter

2023 CURENT Industry Conference
Apr. 2023

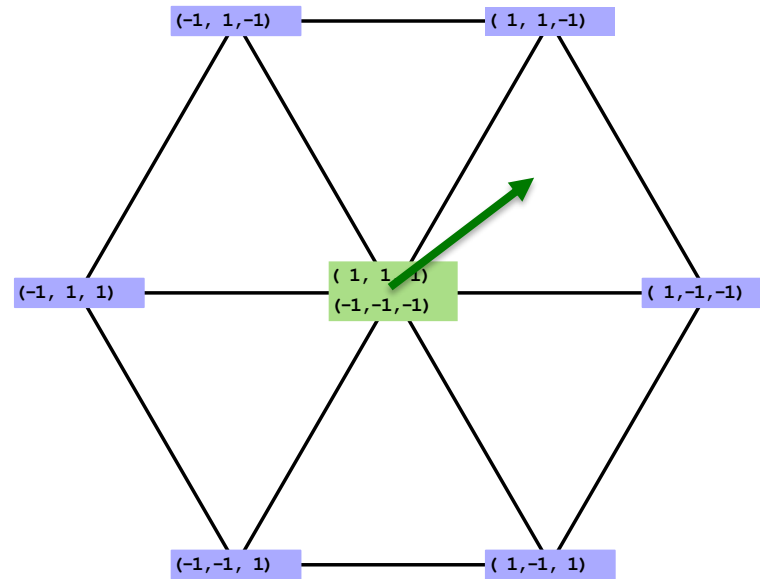
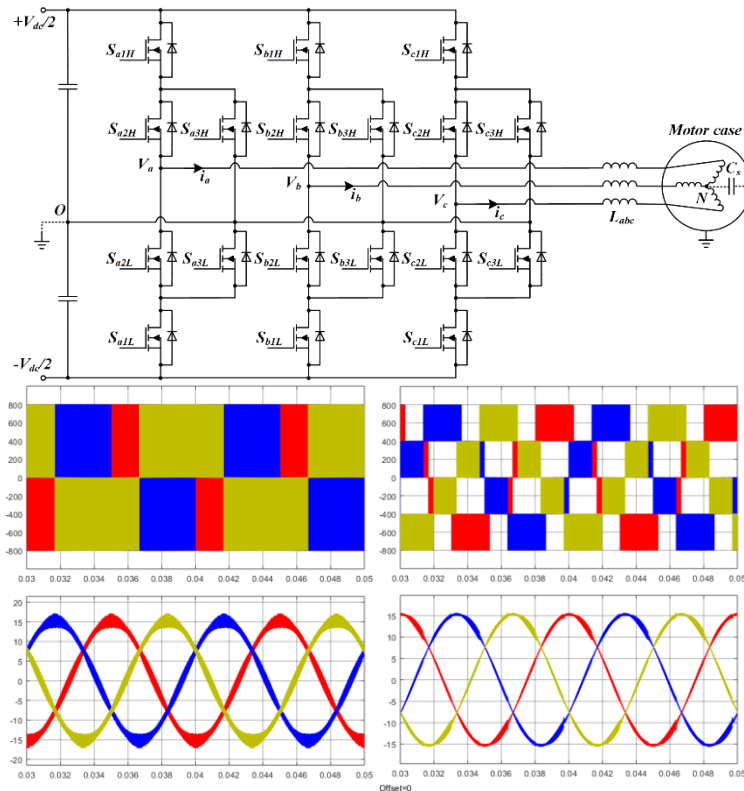
Yang Huang¹, Xin Xia¹, Hua (Kevin) Bai¹
Fanning Jin², Xiaodong Shi², Bing Cheng²

¹University of Tennessee, Knoxville

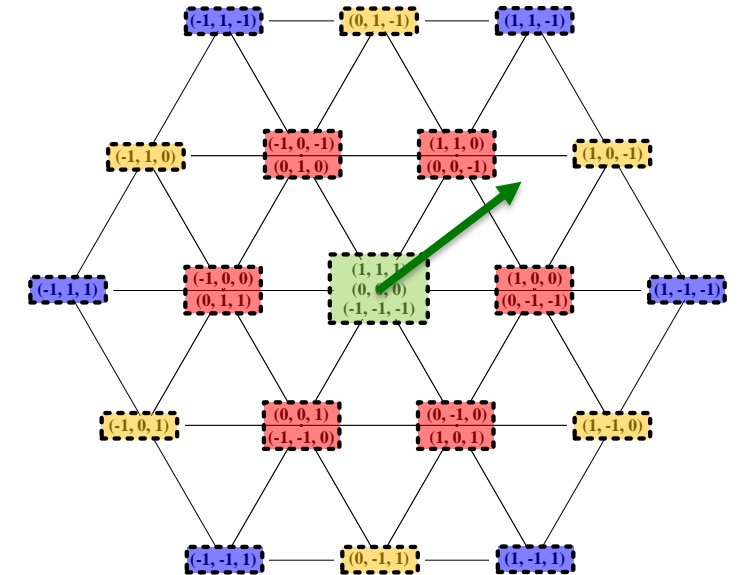
²Mercedes Benz Research and Development North America

Three-level ANPC Realization

- ❑ To have comparable travel time as petrol-driven vehicles, extreme fast charging is promoted. This requires at least 800 V DC-link voltage, which also increase the efficiency.
- ❑ Three-level is preferred for the lower cost of devices with lower voltage blocking capability, especially wide bandgap devices like GaN HEMTs.



2L Vector Plane



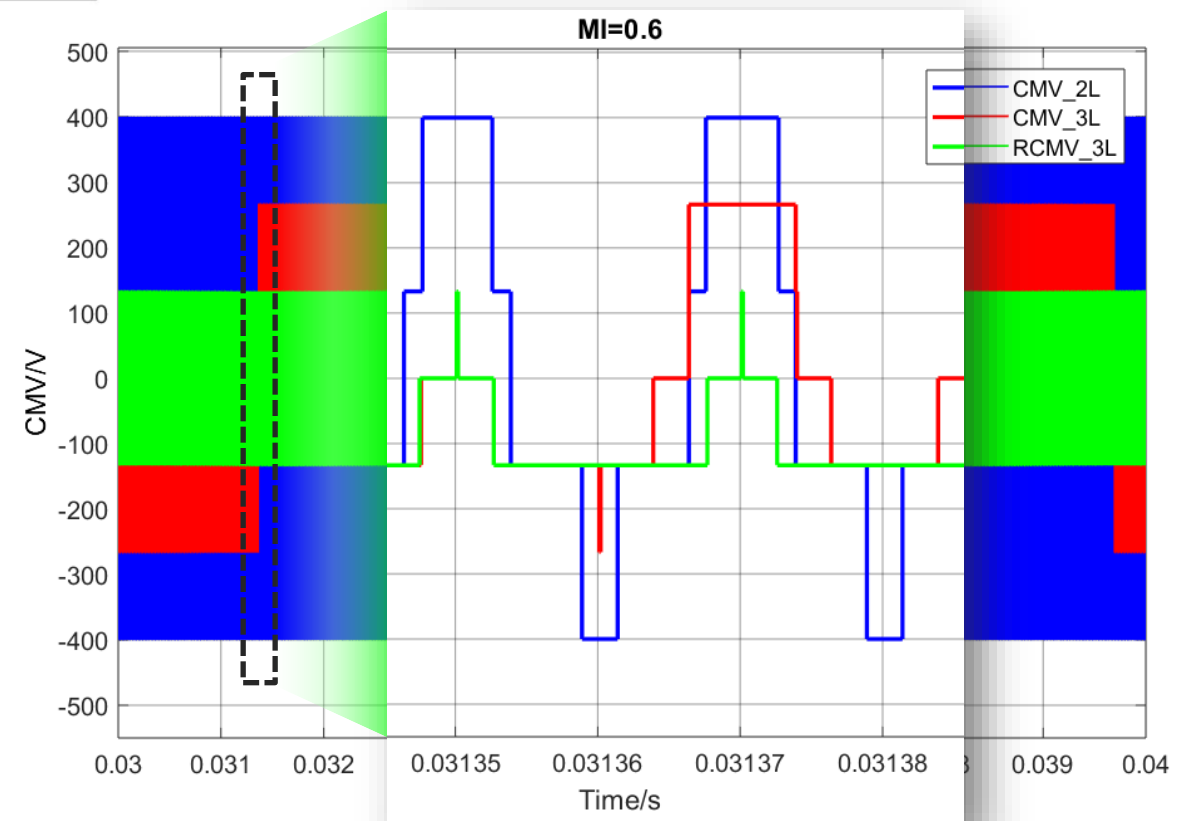
3L Vector Plane

Three-level ANPC Common-mode Voltage

- ❑ Since higher battery voltage directly increase the CMV, combined with higher switching speed, CM current is also larger, causing potentially bigger mechanical damage to the motor.
- ❑ By properly assigning the space vector combination, the CMV can be reduced even more.

$$V_{CM} = \frac{(V_{ao} + V_{bo} + V_{co})}{3}$$

Vector Types	Space Vectors	CMV
Zero voltage vectors	(0, 0, 0)	0
	(1, 1, 1) (-1, -1, -1)	$ V_{dc}/2 $
Small voltage vectors	(1, 1, 0) (1, 0, 1) (0, 1, 1) (-1, -1, 0) (-1, 0, -1) (0, -1, -1)	$ V_{dc}/3 $
	(1, 0, 0) (0, 1, 0) (0, 0, 1) (-1, 0, 0) (0, -1, 0) (0, 0, -1)	$ V_{dc}/6 $
Medium voltage vectors	(1, 0, -1) (0, 1, -1) (-1, 1, 0) (-1, 0, 1) (0, -1, 1) (1, -1, 0)	0
Large voltage vectors	(1, -1, -1) (1, 1, -1) (-1, 1, -1) (-1, 1, 1) (-1, -1, 1) (1, -1, 1)	$ V_{dc}/6 $



Double Fourier Integral Analysis

- ❑ Double Fourier integral analysis can provide analytical solutions to identify harmonic components of the PWM signal.
- ❑ Functions $x(t)$ and $y(t)$ are the time variation of high-frequency carrier waveform and low-frequency modulation waveform.

$$x(t) = \omega_s t + \theta_s$$

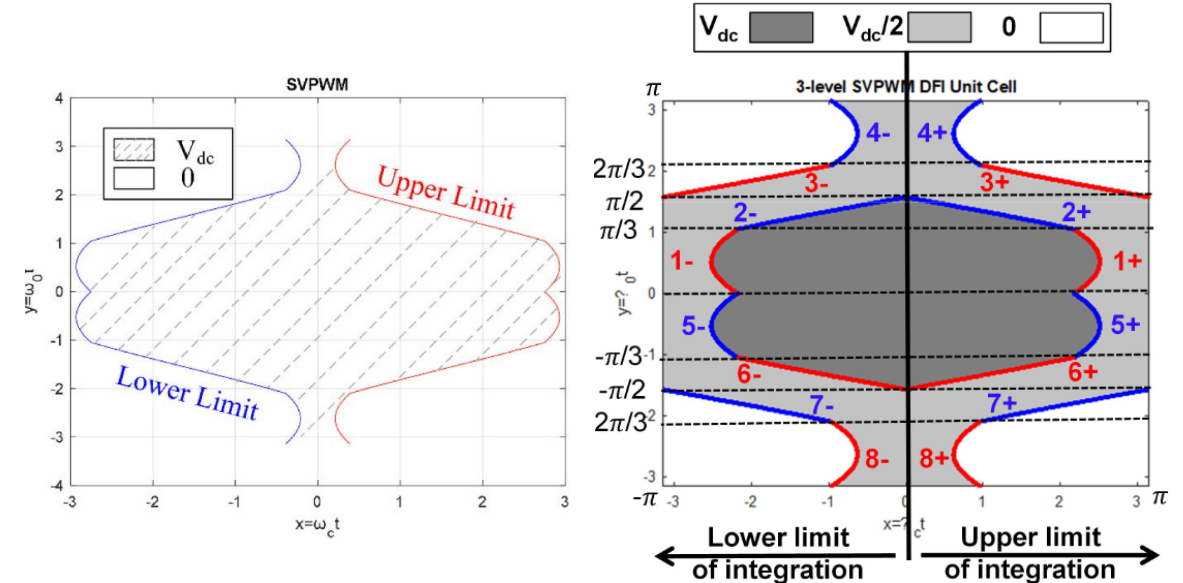
$$y(t) = \omega_0 t + \theta_0$$

Switching function:

$$f(x, y) = \frac{A_{00}}{2} + \sum_{n=1}^{\infty} \left\{ A_{0n} \cos(n(\omega_0 t + \theta_0)) + B_{0n} \sin(n(\omega_0 t + \theta_0)) \right\}$$

$$+ \sum_{m=1}^{\infty} \left\{ A_{m0} \cos(m(\omega_s t + \theta_s)) + B_{m0} \sin(m(\omega_s t + \theta_s)) \right\}$$

$$+ \sum_{m=1}^{\infty} \sum_{\substack{n=-\infty \\ n \neq 0}}^{\infty} \left\{ A_{mn} \cos(m(\omega_s t + \theta_s) + n(\omega_0 t + \theta_0)) + B_{mn} \sin(m(\omega_s t + \theta_s) + n(\omega_0 t + \theta_0)) \right\}$$



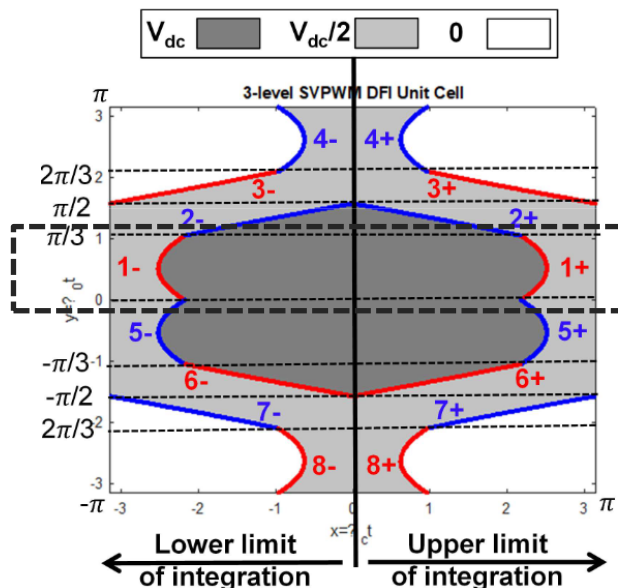
2L Integral Bounds

3L Integral Bounds

Continuous SVM

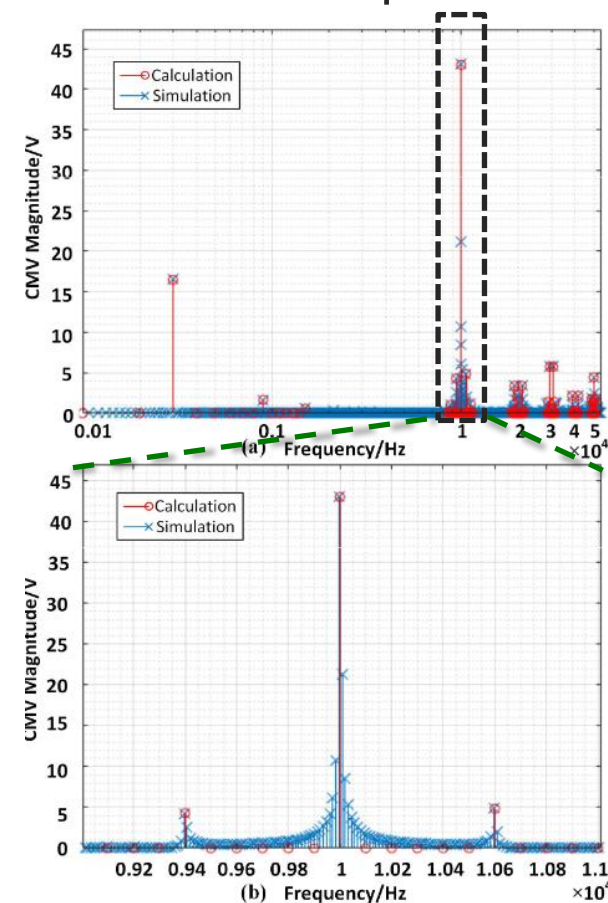
Three-level DFI

- There are 8 sections for each fundamental cycle. Especially, in sections 1, 2, 5, and 6, there are three integration areas. In sections 3, 4, 7, and 8, there is only one.
- The carrier harmonics and sideband components of the CMV can be calculated and compared to the simulation at $f_0=100$ Hz, $f_s=10$ kHz, 200V DC bus voltage.



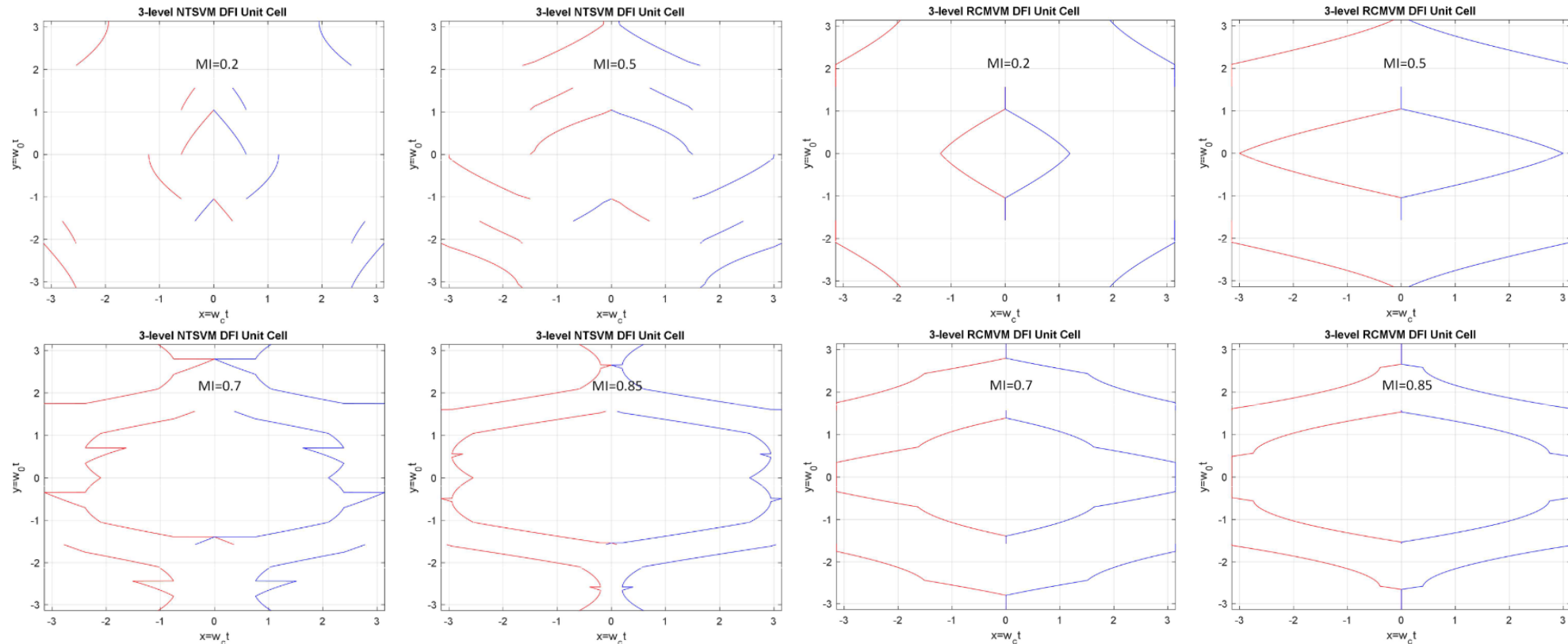
3L Integral Bounds

$$\begin{aligned}
 A_{mn} + jB_{mn} &= \frac{1}{2\pi} \int_{-\pi}^{\pi} \int_{\text{lowerlimit}}^{\text{upperlimit}} \int_{\text{insectori}} U e^{j(mx+ny)} dx dy \\
 &= \int_{-\pi}^{-\frac{2\pi}{3}} \int_{\frac{8-}{8-}}^{\frac{8+}{8-}} \frac{V_{dc}}{2} e^{j(mx+ny)} V_{dc} dx dy + \int_{-\frac{2\pi}{3}}^{-\frac{\pi}{3}} \int_{\frac{7-}{7-}}^{\frac{7+}{7-}} \frac{V_{dc}}{2} e^{j(mx+ny)} V_{dc} dx dy \\
 &+ \int_{-\frac{\pi}{3}}^{-\frac{\pi}{2}} \int_{\frac{6-}{6-}}^{\frac{6+}{6-}} \frac{V_{dc}}{2} e^{j(mx+ny)} V_{dc} dx dy + \int_{-\frac{\pi}{2}}^{-\frac{\pi}{3}} \int_{\frac{6-}{6-}}^{\frac{6+}{6-}} V_{dc} e^{j(mx+ny)} V_{dc} dx dy + \int_{-\frac{\pi}{2}}^{-\frac{\pi}{3}} \int_{\frac{6+}{6+}}^{\frac{6-}{6+}} \frac{V_{dc}}{2} e^{j(mx+ny)} V_{dc} dx dy \\
 &+ \int_{-\frac{\pi}{2}}^{-\frac{\pi}{3}} \int_{\frac{5-}{5-}}^{\frac{5+}{5-}} \frac{V_{dc}}{2} e^{j(mx+ny)} V_{dc} dx dy + \int_{-\frac{\pi}{2}}^{-\frac{\pi}{3}} \int_{\frac{5-}{5-}}^{\frac{5+}{5-}} V_{dc} e^{j(mx+ny)} V_{dc} dx dy + \int_{-\frac{\pi}{2}}^{-\frac{\pi}{3}} \int_{\frac{5+}{5+}}^{\frac{5-}{5+}} \frac{V_{dc}}{2} e^{j(mx+ny)} V_{dc} dx dy \\
 &+ \int_{-\frac{\pi}{3}}^{-\frac{\pi}{2}} \int_{\frac{1-}{1-}}^{\frac{1+}{1-}} \frac{V_{dc}}{2} e^{j(mx+ny)} V_{dc} dx dy + \int_{-\frac{\pi}{3}}^{-\frac{\pi}{2}} \int_{\frac{1-}{1-}}^{\frac{1+}{1-}} V_{dc} e^{j(mx+ny)} V_{dc} dx dy + \int_{-\frac{\pi}{3}}^{-\frac{\pi}{2}} \int_{\frac{1+}{1+}}^{\frac{1-}{1+}} \frac{V_{dc}}{2} e^{j(mx+ny)} V_{dc} dx dy \\
 &+ \int_{-\frac{\pi}{2}}^{-\frac{\pi}{3}} \int_{\frac{2-}{2-}}^{\frac{2+}{2-}} \frac{V_{dc}}{2} e^{j(mx+ny)} V_{dc} dx dy + \int_{-\frac{\pi}{2}}^{-\frac{\pi}{3}} \int_{\frac{2-}{2-}}^{\frac{2+}{2-}} V_{dc} e^{j(mx+ny)} V_{dc} dx dy + \int_{-\frac{\pi}{2}}^{-\frac{\pi}{3}} \int_{\frac{2+}{2+}}^{\frac{2-}{2+}} \frac{V_{dc}}{2} e^{j(mx+ny)} V_{dc} dx dy \\
 &+ \int_{-\frac{2\pi}{3}}^{-\frac{\pi}{3}} \int_{\frac{3-}{3-}}^{\frac{3+}{3-}} \frac{V_{dc}}{2} e^{j(mx+ny)} V_{dc} dx dy + \int_{-\frac{2\pi}{3}}^{-\frac{\pi}{3}} \int_{\frac{4-}{4-}}^{\frac{4+}{4-}} \frac{V_{dc}}{2} e^{j(mx+ny)} V_{dc} dx dy
 \end{aligned}$$



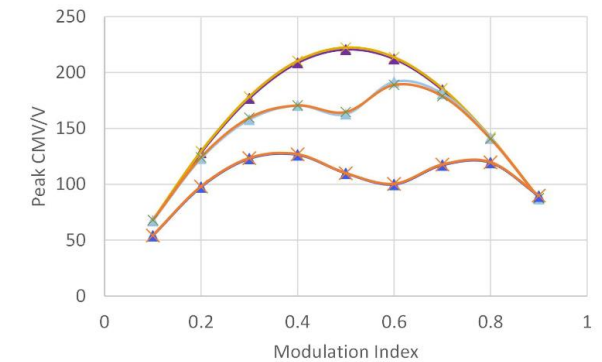
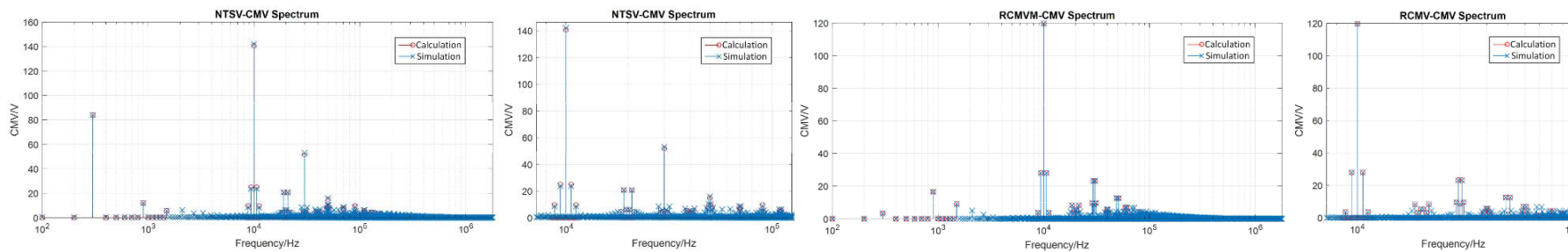
DFI Bounds of Other 3L Modulations

- ❑ NTSVM is nearest three vector modulation. It uses three nearby vectors to compose the reference. RCMVM is reduced common-mode voltage modulation. It always uses low CMV vectors instead.
- ❑ By deriving the switching function, the DFI bounds with different MI can be plotted as below.

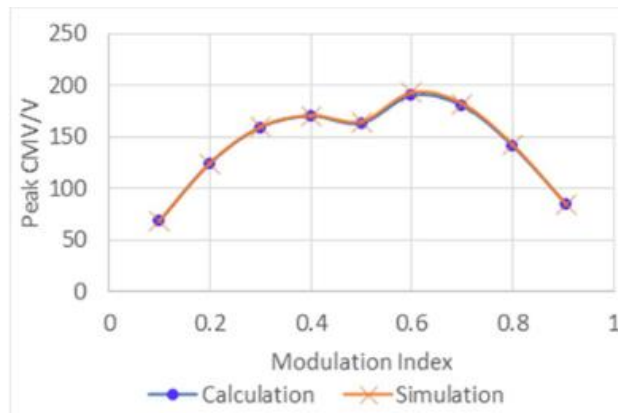


Result Comparison

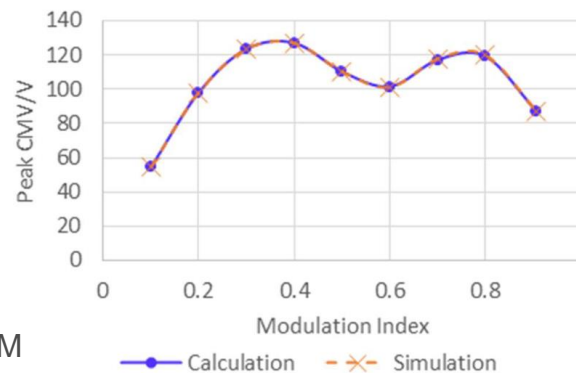
- ❑ Analytical CMV spectrum and the simulation result are compared below.
- ❑ At given DC bus voltage of 800 V, MI=0.8, fs=10 kHz and f0=100 Hz, the result shows very accurate agreement. (left and middle)
- ❑ This result is then compared to preliminary experiment test. (right)



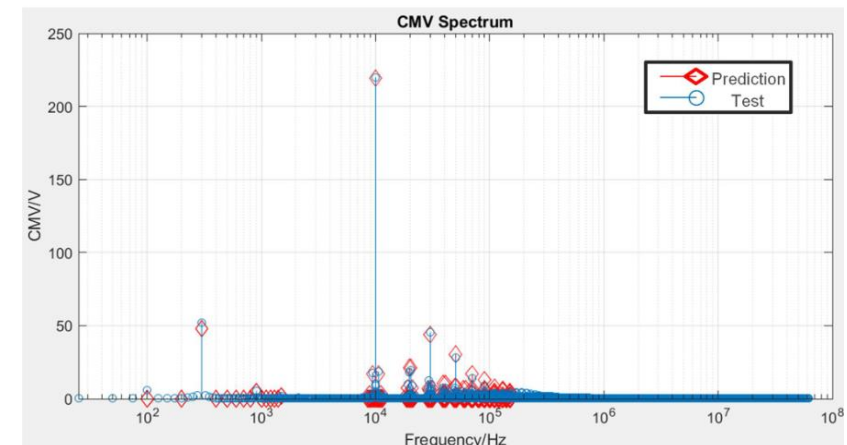
▲ Test/CSVM ▲ Prediction/CSVM
 ▲ Test/NTSVM ▲ Prediction/NTSVM
 ▲ Test/RCMVM ▲ Prediction/RCMVM



NTSVM
←===

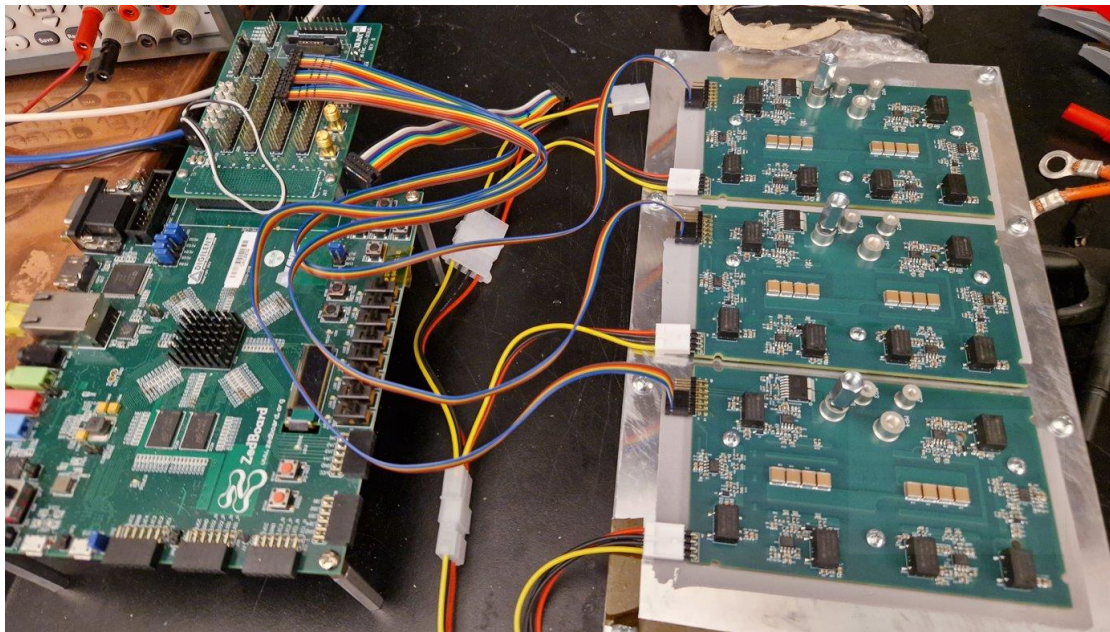


====>
RCMVM

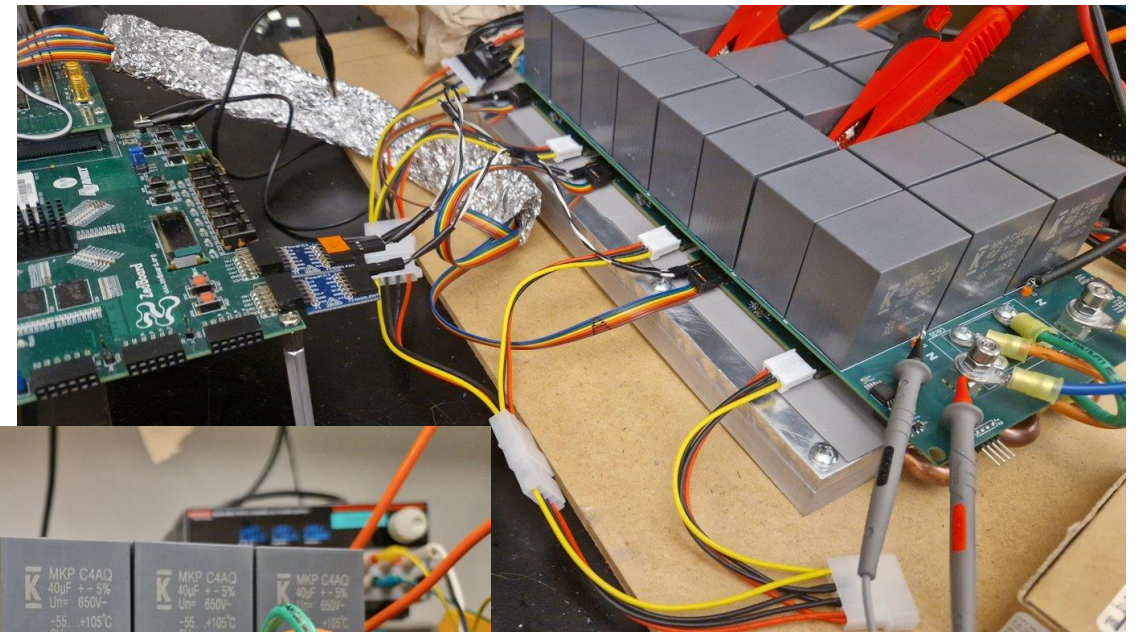


Test Platform

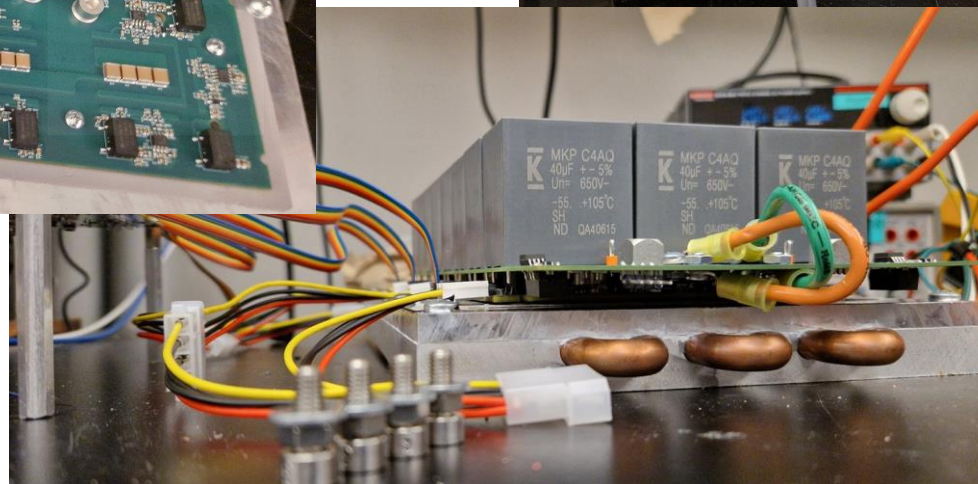
- ❑ Currently, we have built an 800 V, 75 kVA three-level all GaN inverter, with a power density of 25 kVA/L. Tests are conducting to gradually reach full power.
- ❑ More tests are on the way to prove the accuracy of our analytical calculation.



Modular Design Sitting on the Cold Plate



Complete Inverter Connected with FPGA



Low Profile Design

Acknowledgements

*This work was supported by ***.*